Journal of Biomedical Optics

BiomedicalOptics.SPIEDigitalLibrary.org

Multiphoton microscopy as a diagnostic imaging modality for pancreatic neoplasms without hematoxylin and eosin stains

Youting Chen
Jing Chen
Hong Chen
Zhipeng Hong
Xiaoqin Zhu
Shuangmu Zhuo
Yanling Chen
Jianxin Chen

SPIE.

Multiphoton microscopy as a diagnostic imaging modality for pancreatic neoplasms without hematoxylin and eosin stains

Youting Chen,[a] Jing Chen,[b] Hong Chen,[c] Zhipeng Hong,[a] Xiaoqin Zhu,[b,*] Shuangmu Zhuo,[b] Yanling Chen,[d,*] and Jianxin Chen[b]

[a]The First Affiliated Hospital of Fujian Medical University, Department of Hepatobiliary Surgery, Fuzhou 350005, China
[b]Fujian Normal University, Key Laboratory of OptoElectronic Science and Technology for Medicine of Ministry of Education, Fujian Provincial Key Laboratory for Photonics Technology, Institute of Laser and Optoelectronics Technology, Fuzhou 350007, China
[c]The First Affiliated Hospital of Fujian Medical University, Department of Pathology, Fuzhou 350005, China
[d]The Affiliated Union Hospital of Fujian Medical University, Department of Hepatobiliary Surgery, Fuzhou 350001, China

Abstract. Hematoxylin and eosin (H&E) staining of tissue samples is the standard approach in histopathology for imaging and diagnosing cancer. Recent reports have shown that multiphoton microscopy (MPM) provides better sample interface with single-cell resolution, which enhances traditional H&E staining and offers a powerful diagnostic tool with potential applications in oncology. The purpose of this study was to further expand the versatility of MPM by establishing the optical parameters required for imaging unstained histological sections of pancreatic neoplasms, thereby providing an efficient and environmentally sustainable alternative to H&E staining while improving the accuracy of pancreatic cancer diagnoses. We found that the high-resolution MPM images clearly distinguish between the structure of normal pancreatic tissues compared with pancreatic neoplasms in unstained histological sections, and discernable differences in tissue architecture and cell morphology between normal versus tumorigenic cells led to enhanced optical diagnosis of cancerous tissue. Moreover, quantitative assessment of the cytomorphological features visualized from MPM images showed significant differences in the nuclear–cytoplasmic ratios of pancreatic neoplasms compared with normal pancreas, as well as further distinguished pancreatic malignant tumors from benign tumors. These results indicate that the MPM could potentially serve as an optical tool for the diagnosis of pancreatic neoplasms in unstained histological sections. [DOI: 10.1117/1.JBO.19.9.096008]

Keywords: multiphoton microscopy; optical diagnosis; pancreatic neoplasms; unstained histological sections.

Paper 140248RR received Apr. 20, 2014; revised manuscript received Aug. 8, 2014; accepted for publication Aug. 11, 2014; published online Sep. 12, 2014.

1 Introduction

Pancreatic cancer is a lethal malignancy with its incidence almost equivalent to mortality.[1] According to the National Cancer Institute statistics for 2013, 45,220 Americans (22,740 male and 22,480 female) are diagnosed with pancreatic cancer, resulting in 38,460 deaths (19,480 male and 18,980 female).[2] In the US, pancreatic cancer is the tenth most common cancer in terms of incidence but the fourth most common cause of cancer-related deaths. The symptoms of pancreatic tumors, including abdominal or back pain, weight loss, jaundice (yellowing of the skin and eyes), loss of appetite, nausea, light stool color, and diabetes, are usually so generic and common that a clear diagnosis is difficult to make.[3] Moreover, as a disease characterized by nonspecific symptoms, pancreatic cancer often remains undiagnosed until it has reached an advanced stage of malignancy, leading to poor outcomes. Prognosis of pancreatic cancer is unfavorable, since most patients (80% to 85%) are diagnosed with late-stage disease when surgical resections are not possible.[4] Therefore, it is imperative to better understand the fundamental changes in pancreatic cancer in order to develop early diagnostic markers that could improve the survival outcomes for this disease.

Histological examination of pancreatic neoplasms allows the clinicians to macroscopically visualize, diagnose, and grade potential malignancies in pancreatic cancer patients. At present, histopathological examination of hematoxylin and eosin (H&E) stained sections is the standard approach for diagnosis of pancreatic neoplasms. In Harris H&E staining, histological sections are first stained with hematoxylin, which is an oxidizing agent.[5] Eosin is then applied to the section, which is an anionic dye staining almost all proteins and provides contrast for nearly every structure within the tissue. There are two main disadvantages of the H&E staining method in pathology. First, the technical limitations of over or understaining may lead to false coloration of the cytoplasm or nucleus and subsequently lower the contrast and resolution during imaging.[6,7] Second, the oxidizing agent used in H&E staining requires special disposal and is not environmentally sustainable. The development and application of a novel diagnostic imaging modality that obtains images of comparable resolution and quality as standard H&E-stained images will extraordinarily benefit the medical community.

During the past two decades, multiphoton microscopy (MPM) has become a novel optical tool of choice for imaging tissue architecture and cellular morphology.[8–12] The technology

*Address all correspondence to: Xiaoqin Zhu, E-mail: zhuxq@fjnu.edu.cn; Yanling Chen, E-mail: chenyanling1381@126.com

0091-3286/2014/$25.00 © 2014 SPIE

behind MPM is based on nonlinear optical processes such as two or three photon-excited fluorescence (PEF) and second or third harmonic generation. Early studies quantified autofluorescent biomarkers, such as collagen or redox materials such as nicotinamide adenine dinucleotide (phosphate) [NAD(P)H] and flavin adenine dinucleotide (FAD), to characterize the extent of tissue pathology.[13–17] Based on the quantification of NAD(P)H and FAD autofluorescence, MPM has been used to examine the metabolic mechanisms of pancreatic tissues.[18,19] In addition, label-free MPM was also demonstrated to be an efficient tool for observing dynamic cellular events under physiological conditions, allowing detailed characterization of pancreatic pathologies from observed tissue and cellular morphologies.[20,21] Recently, MPM was used to image H&E-stained pathological sections that fluoresce due to the two PEF (TPEF) signal of H&E dyes, demonstrating the potential of MPM to be applied in other histological applications such as cancer imaging and diagnostics that require single-cell resolution.[22] Moreover, it was shown to be effective in imaging unstained tissue slices for the diagnosis of oesophageal cancer.[23]

The purpose of this study is to establish the optical parameters required for imaging and diagnosis of pancreatic neoplasms without H&E staining, specifically using MPM and unstained histological sections from our tissue library. We applied MPM to study samples obtained from normal pancreatic tissue and three types of pancreatic neoplasms. The nuclear–cytoplasmic (N/C) ratio of the normal or neoplastic cells was measured to quantitatively assess differences in cellular morphology. The MPM results were compared with results from standard H&E staining, demonstrating the effectiveness and accuracy of label-free MPM imaging as a diagnostic tool and potential alternative for H&E staining. The absence of histopathological staining procedures would offer an efficient and cost-effective solution for diagnostic laboratories looking to implement environmentally sustainable methodologies. In addition, MPM provides a powerful tool for retrospective analysis of pancreatic tumorigenesis, which may reveal potential morphological features that lead to early diagnosis and improved outcomes for treatment of this fatal disease.

2 Materials and Methods

2.1 *Study Design*

The goals of our study were to expand the applicability of MPM as a diagnostic tool through development of a new methodological approach and to apply that approach in the optical diagnosis of pancreatic neoplasms. To accomplish the first goal, we determined whether the structure of normal pancreatic tissue can be identified in MPM images of unstained histological sections as clearly as in the corresponding H&E-stained samples. The second goal of the study was to test the applicability of the new methodology in a diagnostic setting, probing whether multiphoton imaging of unstained samples can optically distinguish between three types of pancreatic neoplasms as well as H&E-stained tissue samples and lead to an accurate diagnosis.

2.2 *Sample Preparation*

In our study, pancreatic neoplasms embedded in paraffin were provided by the First Affiliated Hospital of Fujian Medical University (Fuzhou, China). Samples included 25 cases of pancreatic neoplasm (9 pancreatic mucinous cystic neoplasm, 10 pancreatic ductal adenocarcinoma, and 6 pancreatic colloid carcinoma), as well as 10 normal pancreatic tissue samples excised 2 cm beyond the resection margins. The samples were collected from patients undergoing a pancreatectomy between July 2008 and August 2012, and postsurgical sample processing involved fixation in formalin, dehydration by alcohol, and embedding in a block of paraffin wax for preservation. Prior to MPM imaging, four sections of 5-μm thickness were sliced from each paraffin block sample by a microtome. Each section was deparaffinized with xylene and rehydrated with a series of alcohol washes, and the processed samples were sandwiched between a microscope slide and cover glass for MPM imaging. After MPM imaging, the sections were stained with H&E stains according to standard procedures for histological examination with standard light microscopy.[24] MPM images and H&E-stained images were compared and analyzed by two certified pathologists.

2.3 *MPM Imaging Instrumentation*

The multiphoton imaging system used in this study contained a high-throughput scanning inverted Axiovert 200 microscope (LSM 510 META; Zeiss, Oberkochen, Baden-Württemberg, Germany) and a mode-locked femtosecond Ti:sapphire laser (110 fs, 76 MHz) tunable from 700 to 980 nm (Mira 900-F; Coherent, Santa Clara, California).[23,25] For high-resolution imaging, a Plan-Neofluar objective (40× and NA = 0.75, Zeiss) was employed in MPM examination. The excitation wavelength (λ_{ex}) used in this study was 810 nm.

Previously, we found that the histological sample processing enhanced the TPEF signal of cytoplasm and nucleoli in epithelial cells and collagen in stromal cells, but destroyed the noncentrosymmetric molecular structure of collagen resulting in loss of the intrinsic second-harmonic generation signal.[23] In addition, we found that the sample processing also led to the loss of NAD(P)H and FAD, which destroyed the TPEF signals that can be used as standard biomarkers of epithelium and whose fluorescence ratio (redox ratio) was indicative of the cellular metabolic state.

To account for these alterations in emission signals caused by histological sample processing, the image acquisition channel 3 under single-track channel mode setting was used to collect multiphoton emission signals in this study. In the optical path, a main dichroic beam splitter (KP650) was set in order to separate the emissions from the excitation light, and BG-39 glass was selected as second dichroic beam splitter in order to block any stray excitation light. The emission light was detected in the wavelength range between 350 and 710 nm by a photon counting photomultiplier tube module. Large-area images were obtained by using an optional HRZ 200 fine-focusing stage (HRZ 200; Carl Zeiss, Inc., Oberkochen, Baden-Württemberg, Germany). All images had a 12-bit pixel depth. The images were obtained at 2.56-μs/pixel.

The light microscope used for imaging H&E-stained sections was a standard bright field light microscope (Eclipse Ci-L, Nikon Instruments Inc., Tokyo, Japan) with a CCD camera (Nikon, DS-Fi2, Japan). An objective (Plan-fluor 40×, Nikon) was used in histological examination.

2.4 *Quantification of Morphological Features*

To quantitatively assess the differences in morphological features between normal and three types of pancreatic neoplastic tissues, the N/C ratio was defined as the measurement of the

size of the nucleus in relation to the area of the cytoplasm within cells of each tissue. Five random fields in each MPM image were selected, and cells within each field were quantified. Cells with cytoplasm and nuclei demonstrating complete and clearly discernable outlines were chosen, circled, and measured using an optional fine-focusing stage (HRZ 200 stage, Carl Zeiss). N/C ratios were expressed as the mean value followed by its standard deviation (mean $\pm$ SD). In addition, the N/C ratios were measured again following H&E staining to verify the reliability of the MPM technique.

When quantifying the morphological features of pancreatic epithelium, the localization and function of each cell were taken into account so that the comparisons would be made between similar cells. For example, acinar epithelial cells and ductal epithelial cells had striking morphological differences due to their unique functions within the pancreas.[26] Pancreatic colloid carcinoma was a kind of acinar-derived cancer, and pancreatic mucinous cystic neoplasm or pancreatic ductal adenocarcinoma was a kind of ductal-derived cancer. In this study, the colloid-producing epithelial cells in pancreatic colloid carcinoma (acinar-derived) were compared with acinar epithelial cells from a normal pancreas. The mucin-producing epithelial cells in pancreatic mucinous cystic neoplasm (ductal-derived) and cancerous ductal epithelial cells in pancreatic ductal adenocarcinoma (ductal-derived) were compared with ductal epithelial cells from a normal pancreas.

Datasets were analyzed using the Shapiroe–Wilk test, and results followed a Gaussian distribution when the *P*-value was greater than 0.05. The one-way ANOVA and least-significant difference analyses were used to determine statistically significant differences in the ratios of N/C between normal and neoplastic tissues and between benign and malignant tumors. Statistical analysis was performed using SPSS software (version 16.0). Exact *P*-values were computed, and differences were considered to be statistically significant when the *P*-values were less than 0.05.

3 Results

3.1 *Patient Demographics and Specimen Characteristics*

Normal pancreatic tissues from 10 patients were analyzed and compared with pancreatic neoplasms from 25 patients in this pilot study. The patient demographics and neoplastic characteristics were summarized in Table 1.

3.2 *MPM Diagnostic Features of Normal Pancreas*

In total, 36 sections of pancreatic mucinous cystic neoplasm, 40 sections of pancreatic ductal adenocarcinoma, 24 sections of pancreatic colloid carcinoma, and 40 sections of normal pancreatic samples were examined using MPM by detecting the peak multiphoton fluorescence intensity. A representative MPM image of the normal tissue was shown in Fig. 1(a), revealing regular tissue architecture and cell morphology. It clearly presented the typical arrangement of normal architecture of pancreatic acinus [dashed line in Fig. 1(a)] and pancreatic duct [solid line in Fig. 1(a)]. Concentric fibrous bundles were observed around the ducts with occasionally short and thick collagen fibers [pentagram in Fig. 1(a)].[27] The acinar cells [dashed arrow in Fig. 1(a)] were uniform and maintained their polarity with no evidence of nuclear overlapping. Also, the bright nucleolus was easily identifiable within the acinar cell. The interlobular duct [dotted line in Fig. 1(a)] was surrounded with fibrous connective tissue, and cuboidal epithelium constituted the ductal walls. These observations of cellular architecture were comparable with the corresponding H&E-stained image shown in Fig. 1(b), where the positions of the pancreatic acinus [dashed line in Fig. 1(b)], pancreatic duct [solid line in Fig. 1(b)], collagen fibers [pentagram in Fig. 1(b)], acinar cells [dashed arrow in Fig. 1(b)], and interlobular duct [dotted line in Fig. 1(b)] were identical to the corresponding positions in the MPM images.

3.3 *MPM Diagnostic Features of Pancreatic Benign Tumor*

The representative large-area MPM image of the pancreatic mucinous cystic neoplasm in Fig. 2(a) showed that the lesion was mainly composed of a single layer of columnar, mucin-producing epithelium [dashed arrow in Fig. 2(a)]. The epithelium was supported by ovarian-type stroma [triangle in Fig. 2(a)]. Occasionally, the dense ovarian-type stroma was replaced by a dense collagenized stroma [pentagram in Fig. 2(a)].[28] The structure of the lesion was rather disordered, while there were blood vessels [dotted arrow in Fig. 2(a)] distributed within the lesion tissue. It was comparable with the corresponding H&E image shown in Fig. 2(b), presenting mucin-producing epithelium [dashed arrow in Fig. 2(b)], ovarian-type stroma [triangle in Fig. 2(b)], collagenized stroma [pentagram in Fig. 2(b)], and blood vessels [dotted arrow in Fig. 2(b)] in identical positions as the MPM image.

Table 1 Patient demographics and tissue characteristics.

Variable	Normal pancreas	Pancreatic mucinous cystic neoplasm	Pancreatic ductal adenocarcinoma	Pancreatic colloid carcinoma
Age (years): median (range)	58 (41 to 75)	55 (46 to 59)	62 (47 to 75)	65 (63 to 69)
Gender (male/female)	5/5	4/5	3/7	1/5
Tumor size (cm): median (range)	—	6 (4 to 9)	3.5 (2.5 to 6)	4 (3 to 5)
Tumor location (head/body/tail)	—	1/0/2	11/0/3	1/0/2
Number of cases	10	9	10	6
Number of sections	40	36	40	24

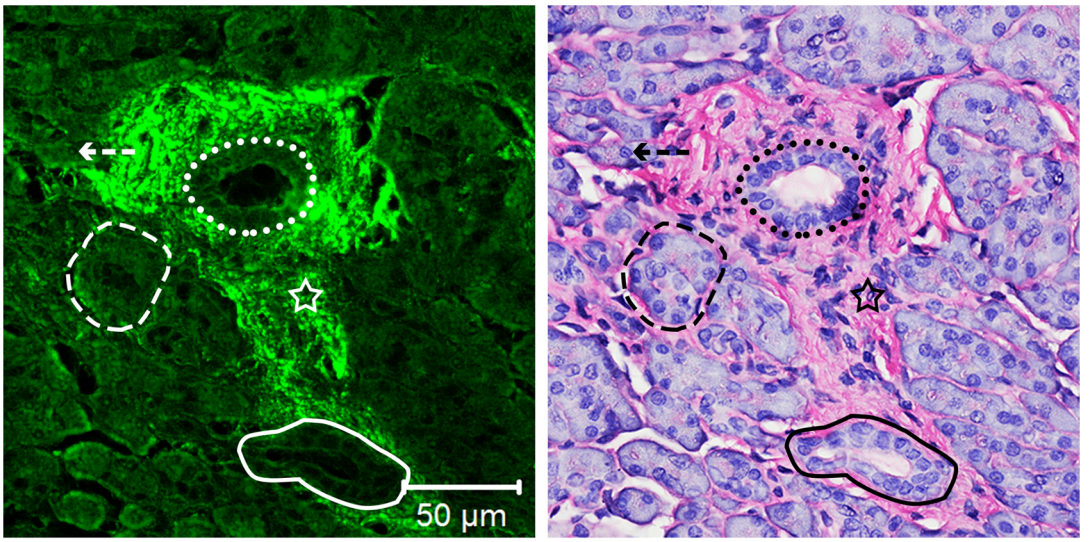

Fig. 1 Comparison of MPM and H&E images in normal pancreatic tissue. (a) The representative MPM image (40×) of an unstained section clearly reveals the normal tissue architecture and cell morphology, including typical organization of pancreatic acinus (dashed line) and pancreatic duct (solid line), the interlobular duct (dotted line), collagen fibers (pentagram), and the acinar cell (dashed arrow). (b) The corresponding H&E image (40×) of fixed, stained pancreatic tissue shows a similar cell arrangement: the pancreatic acinus (dashed line), pancreatic duct (solid line), interlobular duct (dotted line), collagen fibers (pentagram), and the acinar cell (dashed arrow).

3.4 *MPM Diagnostic Features of Pancreatic Malignant Tumors*

The representative large-area MPM image of the pancreatic ductal adenocarcinoma in Fig. 3(a) revealed that the cancer tissue was composed of nonuniform and irregular glands [solid arrows in Fig. 3(a)]. Necrosis [arrow head in Fig. 3(a)] was observed in the glandular cavity. Blood vessels [dotted arrow in Fig. 3(a)] composed of randomly arranged, vascular endothelial cells were observed between the glands. Bands of fibrous stroma surrounding malignant glands and vessels were observed with a marked increase in collagen compared with normal pancreatic tissue [pentagram in Fig. 3(a)]. Deposition of a collagen-rich stroma around a malignant gland may represent a physiologic effort to confine the cancer.[29] More importantly, high-magnification MPM images showed cancer cells concentrated in lesion tissue [dashed arrows in Fig. 3(c)]. Tumorigenic cells displayed

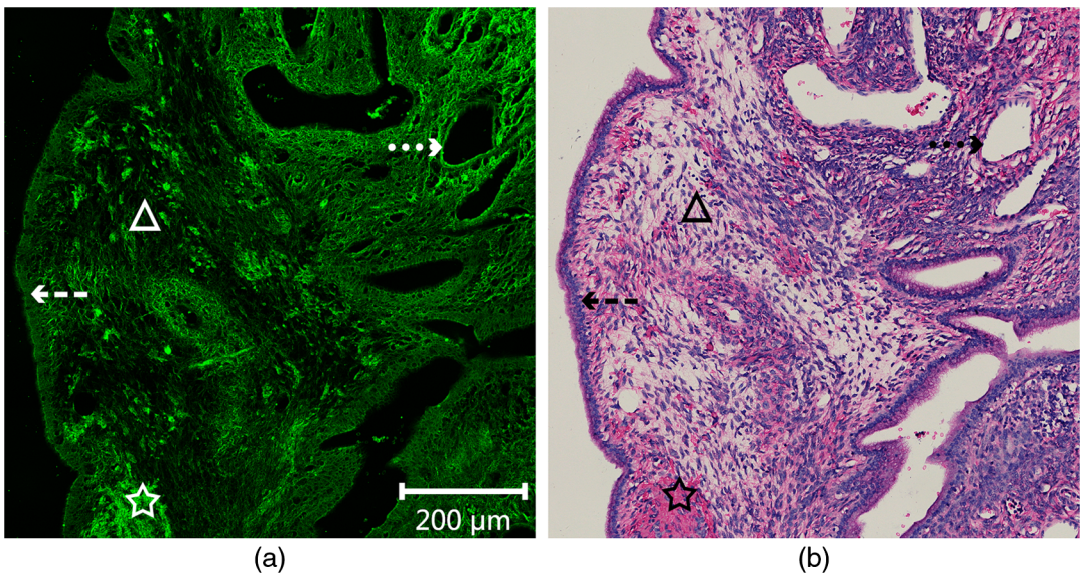

Fig. 2 Comparison of MPM and H&E images in pancreatic mucinous cystic neoplasm. (a) The representative MPM image (10×) of an unstained section reveals a lesion composed of a single layer of columnar, mucin-producing epithelium (dashed arrow), ovarian-type stroma (triangle), collagenized stroma (pentagram), and a blood vessel (dotted arrow). (b) The corresponding H&E image (10×) shows the similar features that correlate with the MPM image: the mucin-producing epithelium (dashed arrow), ovarian-type stroma (triangle), collagenized stroma (pentagram), and a blood vessel (dotted arrow).

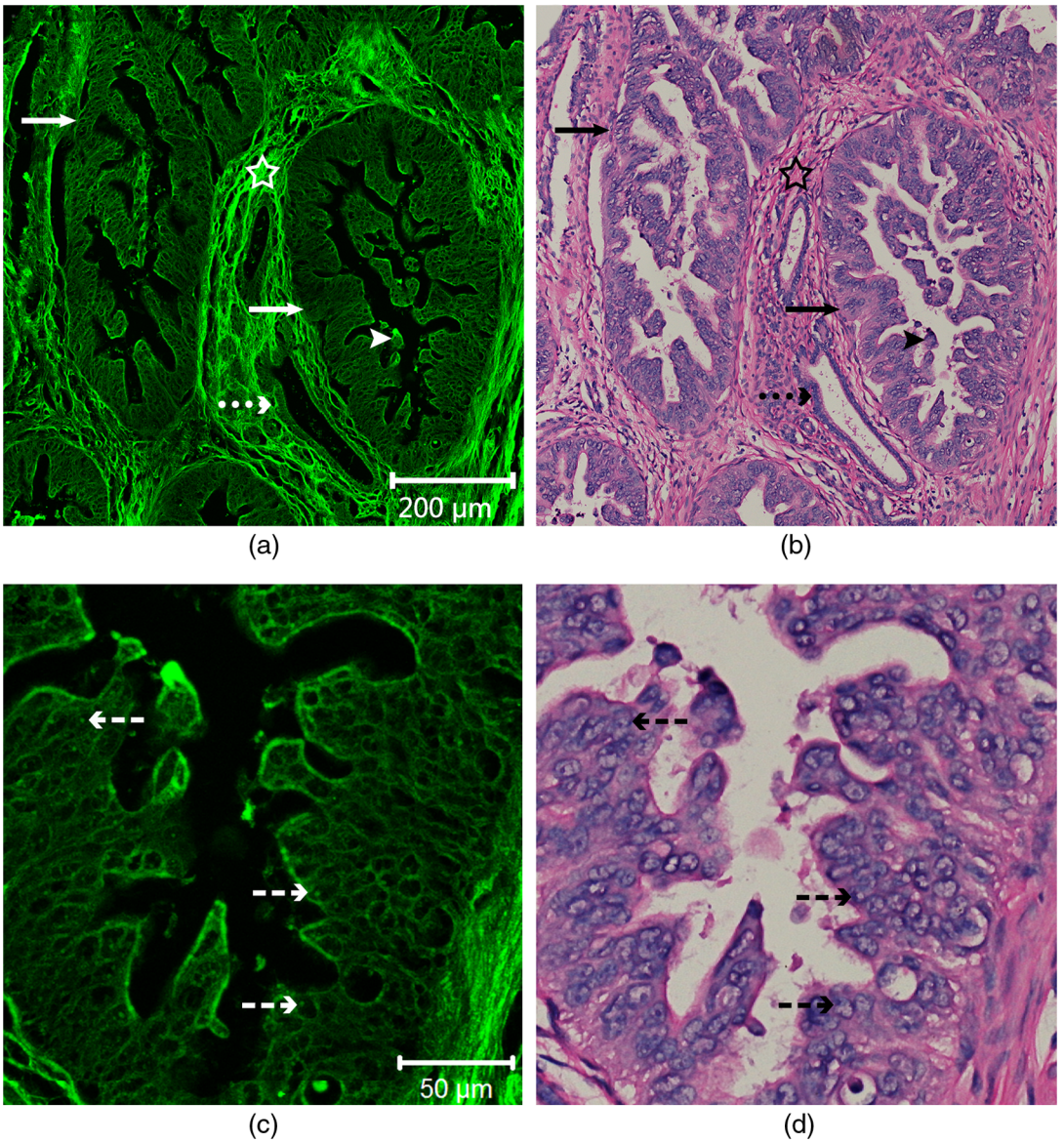

Fig. 3 Comparison of MPM and H&E images in pancreatic ductal adenocarcinoma. (a) The representative MPM image (10×) of an unstained section reveals the irregular glands (solid arrows), necrosis (arrow head), blood vessels (dotted arrow), and collagen fibers (pentagram). (b) The corresponding H&E image (10×) shows the similar features that correspond to the MPM image: irregular glands (solid arrows), necrosis (arrow head), blood vessels (dotted arrow), and collagen fibers (pentagram). (c) Magnified MPM image (40×) presents the cancer cells (dashed arrows) that exhibit distinct cellular features with illustrious nucleoli. (d) The standard bright field light microscopic image (40×) of the corresponding H&E-stained histological section shows cancer cells (dashed arrows) with a similar appearance to the corresponding MPM image.

marked cellular and nuclear pleomorphisms characterized by irregular size and shape, enlarged nuclei and bright nucleoli. Unlike normal pancreatic tissue, the intercellular space between individual cells in malignant tissue was not readily discernable. These features were readily correlated with the corresponding H&E images shown in Figs. 3(b) and 3(d) including the irregular glands [solid arrows in Fig. 3(b)], necrosis [arrow head in Fig. 3(b)], blood vessels [dotted arrow in Fig. 3(b)], collagen fibers [pentagram in Fig. 3(b)], and cancer cells [dashed arrows in Fig. 3(d)].

In the pancreatic colloid carcinoma, the representative large-area MPM image shown in Fig. 4(a) revealed nests of cancer cells [open arrows in Fig. 4(a)] that were sporadically distributed. Glandular expansion was easily discernable [asterisks in Fig. 4(a)], and clusters of cancer cells floated in mucous lakes that were formed by the expanded stroma. Dense bands of collagen [pentagram in Fig. 4(a)] were clearly observed, separating the mucous lakes.[30] At high magnification, cell clusters or "nests" [open arrow in Fig. 4(c)] were composed of a large number of cancer cells [dashed arrow in Fig. 4(c)]. These cancer cells were characterized by irregular size and shape, enlarged nuclei and bright nucleoli. The features were consistent with the H&E-stained results shown in Figs. 4(b) and 4(d), which visualized the nest of cancer [open arrows in Figs. 4(b) and 4(d)], mucous lakes [asterisks in Fig. 4(b)], collagen fibers [pentagram in Fig. 4(b)], and cancer cells [dashed arrow in Fig. 4(d)].

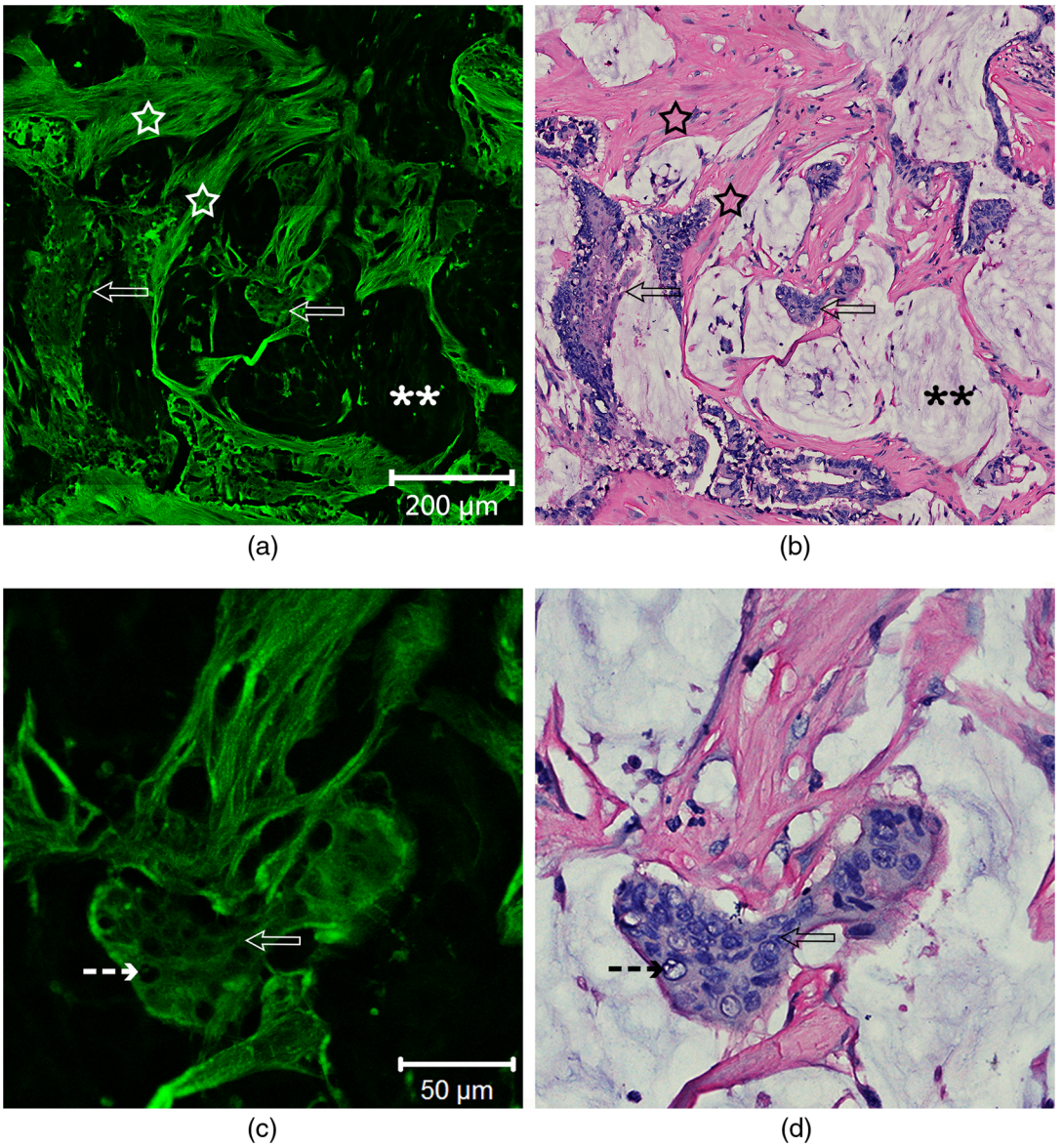

Fig. 4 Comparison of MPM and H&E images in pancreatic colloid carcinoma. (a) The representative MPM image (10×) of an unstained section reveals the nest of cancerous tissue (open arrows), mucous lakes (asterisks), and collagen fibers (pentagrams). (b) The corresponding H&E image (10×) shows the similar features that correlate with the MPM image: the clusters of malignant cells (open arrows), mucous lakes (asterisks), and collagen fibers (pentagrams). (c) Magnified MPM image (40×) demonstrates that the nest of cancerous tissue (open arrow) is formed by a large number of cancer cells (dashed arrow). (d) The corresponding H&E light microscopic image (40×) reveals the similar cellular architecture that correlates with the MPM image: the cluster of malignant tissue (open arrow) containing cancer cells (dashed arrow).

3.5 *Quantitative Analyses of Normal and Neoplastic Pancreatic Tissues*

To quantitatively assess the morphological differences between normal and neoplastic pancreatic cells, a total of 20 cells in five random fields were examined within each MPM image. The N/C ratios from normal pancreatic cells or three types of neoplastic tissues were calculated and analyzed (Fig. 5). The N/C ratio was 0.25 ± 0.05 ($N = 40$) in normal pancreatic acinar epithelium cells, but the ratio increased to 0.85 ± 0.04 ($N = 24$) in colloid-producing epithelium cells found in pancreatic colloid carcinomas. The N/C ratio was 0.48 ± 0.04 ($N = 40$) in normal pancreatic ductal epithelium cells, while it was 0.59 ± 0.05 ($N = 36$) in mucin-producing epithelium cells of pancreatic mucinous cystic neoplasms. However, the N/C ratio increased to 0.72 ± 0.10 ($N = 40$) in cancerous ductal epithelium cells isolated from pancreatic ductal adenocarcinomas. We observed a statistically significant difference between the N/C ratio of pancreatic malignant tumor cells (colloid carcinoma) and normal pancreatic cells (acinus) ($P < 0.001$). In addition, there was a statistically significant increase in the N/C ratio of pancreatic malignant tumors (ductal adenocarcinoma) compared with normal pancreatic cells (duct) ($P < 0.001$) and benign tumors (mucinous cystic neoplasm) ($P < 0.001$). We also observed a statistically significant increase in the N/C ratio of benign tumors (pancreatic mucinous cystic neoplasm)

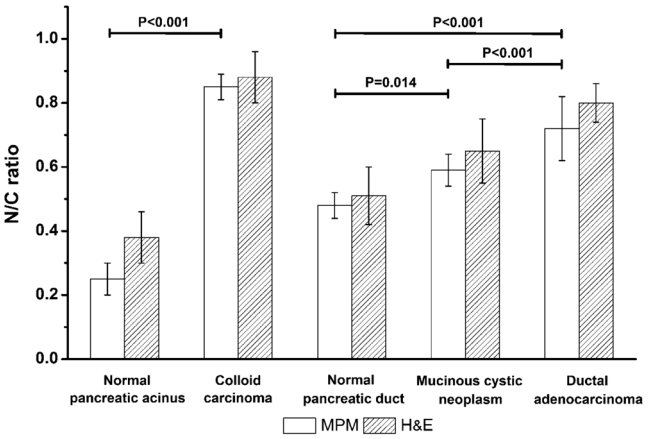

Fig. 5 The N/C ratios of normal tissue and three types of pancreatic neoplasms (mean ± SD) measured from MPM or standard H&E stained images. Error bars indicate standard deviations.

compared with normal pancreatic tissue ($P = 0.014$). These results demonstrate that the N/C ratios obtained from MPM images successfully delineated malignant from normal tissues, with the ratios from malignant tumors being significantly greater than that of the normal pancreas or the pancreatic benign tumors. Quantitative analysis of benign tumors indicated that the N/C ratio was also significantly greater than the ratio of normal pancreas. Together, these data indicated the power of MPM imaging in distinguishing between tumors with differing malignant potential.

The quantitative results of the N/C ratios measured from H&E images were also presented in Fig. 5 for comparison. Similar to the results calculated from MPM images, there was significant difference in the N/C ratios between colloid-producing epithelial cells of pancreatic colloid carcinomas (malignant tumor) and normal pancreatic acinar epithelium cells (compare 0.88 ± 0.08 versus 0.38 ± 0.08, $P < 0.001$). There was also a significant difference in the N/C ratios between cancerous ductal epithelium cells of pancreatic ductal adenocarcinomas (malignant tumor) and normal pancreatic ductal epithelial cells (compare 0.80 ± 0.06 versus 0.51 ± 0.09, $P < 0.001$) or mucin-producing epithelial cells of pancreatic mucinous cystic neoplasms (benign tumor) (compare 0.80 ± 0.06 versus 0.65 ± 0.10, $P < 0.001$). Moreover, a statistically significant difference was also observed between pancreatic mucinous cystic neoplasms (benign tumor) and normal pancreas (compare 0.65 ± 0.10 versus 0.51 ± 0.09, $P < 0.001$). In addition, differences in the N/C ratios between MPM and H&E images were not found to be statistically significant (data not shown).

4 Discussion

4.1 *Feasibility of Using MPM to Diagnose Pancreatic Neoplasms*

Currently, morphological examination of stained histological sections remains the standard diagnostic approach for pancreatic cancer. We performed this study to compare the morphological features of normal pancreas and pancreatic neoplasms based on MPM images of unstained tissues. Our studies showed that the MPM imaging could clearly delineate the parenchyma and the stroma in pancreatic specimens. Specially, it revealed regular tissue architecture and cell morphology in normal pancreas, and distinctive tissular and cellular pleomorphisms in pancreatic neoplasms. More importantly, typical cancer cells, characterized by irregular size and shape and with enlarged nuclei, were clearly observed in MPM images. In short, the high-resolution MPM images clearly demonstrated apparent differences between normal pancreatic tissue and pancreatic neoplasms, as well as distinguished between benign versus malignant tumors in terms of their tissue architecture and cell morphology, and these results were comparable with H&E images.

Moreover, when we quantitatively assessed the N/C ratios obtained from MPM images, we found that the ratios for pancreatic malignant and benign tumors were clearly distinguishable from normal pancreatic tissue. In addition, we were able to distinguish between pancreatic malignant versus benign tumors using the N/C ratios from MPM images. These data were consistent with the H&E results, as well as previous reports that suggest the N/C ratio in neoplastic cells is greater than in normal cells due to the presence of enlarged nuclei that undergo an enhanced rate of mitosis.[31] It was demonstrated that single abnormal cells, irregular nuclear membranes, and enlarged nuclei were important cytologic criteria for differentiating malignant from benign pancreatobiliary specimens.[32] In addition, the extensive activity of the nucleus in neoplastic cells increases with the stage and grade of malignancy, resulting in increased N/C ratios in malignant tumors compared with benign tumors. An increased N/C ratio, marked nuclear envelope abnormalities, prominent nucleoli and hyperchromasia have been demonstrated as overt malignancy.[33]

Furthermore, comparison of the N/C ratios in H&E versus MPM samples showed similar results, which verified the reliability of the MPM technique. Together, these data suggest that the application of MPM for histological investigations of biopsy specimens can be used to reliably diagnose the pancreatic neoplasms in unstained tissue slices.

4.2 *Significance of This Study*

The application of optical methods with single-cell resolution provides detailed characterization of pancreatic morphology and improves the accurate detection and diagnosis of pancreatic neoplasia, which is a significant advancement in the field of histology.[11] Because H&E staining may cause chromatic aberration and produce environmental waste, alternative methods such as MPM imaging of unstained sections may be used to diagnose and classify pancreatic diseases including cancer without the disadvantages associated with traditional histological methods. Another advantage of MPM is its versatility, since it does not require fresh tissue samples and is an excellent tool for retrospective analyses of unstained histological sections acquired over several years. Less is understood regarding the association between early morphological changes within the pancreas and later development of pancreatic cancer, and MPM may help to establish early diagnostic markers through analysis of sample libraries obtained from early and late-stage cancer patients around the world.

In conclusion, we demonstrated that the MPM acquires valuable and complementary information from unstained tissues with the same degree of accuracy as H&E staining. MPM can be successfully used to differentiate between pancreatic neoplasms and normal pancreas, as well as distinguish pancreatic benign tumors from malignant tumors, further establishing its promise as a diagnostic tool. Future studies will utilize MPM imaging to perform a retrospective analysis of unstained

pancreatic tumors obtained from a tissue library, in order to visualize changes in tumor morphology and malignancy over time in single patients.

Acknowledgments

The project was supported by the Program for Changjiang Scholars and Innovative Research Team in University (Grant No. IRT1115), the National Natural Science Foundation of China (Grant Nos. 81101209, 61275006, 81271620, and 61335011), the Natural Science Foundation for Distinguished Young Scholars of Fujian Province (2014J06016), and the China Scholarship Council Funding.

Declaration of Conflicting Interests: The authors declared no potential conflicts of interests with respect to the authorship and/or publication of this article.

References

1. S. Raimondi, P. Maisonneuve, and A. B. Lowenfels, "Epidemiology of pancreatic cancer: an overview," *Nat. Rev. Gastroenterol. Hepatol.* **6**(12), 699–708 (2009).
2. R. Siegel, D. Naishadham, and A. Jemal, "Cancer statistics, 2013," *CA Cancer J. Clin.* **63**(1), 11–30 (2013).
3. S. Kaur et al., "Early diagnosis of pancreatic cancer: challenges and new developments," *Biomarkers Med.* **6**(5), 597–612 (2012).
4. J. Klapman and M. P. Malafa, "Early detection of pancreatic cancer: why, who, and how to screen," *Cancer Control* **15**(4), 280–287 (2008).
5. J. A. Kiernan, *Histological and Histochemical Methods: Theory and Practice*, 3rd ed., Butterworth Heinemann, Woburn (1999).
6. K. Larson et al., "Hematoxylin and eosin tissue stain in Mohs micrographic surgery: a review," *Dermatol. Surg.* **37**(8), 1089–1099 (2011).
7. G. W. Gill, "H&E staining," Chapter 20 in *Education Guide: Special Stains and H&E*, 2nd ed., G. L. Kumar and J. A. Kiernan, Eds., pp. 177–184, Dako North America, Carpinteria, California (2010).
8. W. R. Zipfel et al., "Live tissue intrinsic emission microscopy using multiphoton-excited native fluorescence and second harmonic generation," *Proc. Natl. Acad. Sci. U. S. A.* **100**(12), 7075–7080 (2003).
9. L. E. Grosberg et al., "Spectral characterization and unmixing of intrinsic contrast in intact normal and diseased gastric tissues using hyperspectral two-photon microscopy," *PLoS One* **6**(5), e19925 (2011).
10. P. Steven et al., "Experimental induction and three-dimensional two photon imaging of conjunctiva-associated lymphoid tissue," *Invest. Ophthalmol. Visual Sci.* **49**(4), 1512–1517 (2008).
11. J. N. Rogart et al., "Multiphoton imaging can be used for microscopic examination of intact human gastrointestinal mucosa ex vivo," *Clin. Gastroenterol. Hepatol.* **6**(1), 95–101 (2008).
12. A. Zoumi et al., "Imaging cells and extracellular matrix in vivo by using second-harmonic generation and two-photon excited fluorescence," *Proc. Natl. Acad. Sci. U. S. A.* **99**(17), 11014–11019 (2002).
13. W. Hu et al., "Characterization of collagen fibers by means of texture analysis of SHG images using orientation-dependent gray level co-occurrence matrix method," *J. Biomed. Opt.* **17**(2), 026007 (2012).
14. R. M. Haralick et al., "Textural features for image classification," *IEEE Trans. Syst. Man Cybern.* **3**(6), 610–621 (1973).
15. L. M. Tiede et al., "Determination of hair cell metabolic state in isolated cochlear preparations by two-photon microscopy," *J. Biomed. Opt.* **12**(2), 021004 (2007).
16. N. D. Kirkpatrick et al., "Endogenous optical biomarkers of ovarian cancer evaluated with multiphoton microscopy," *Cancer Epidermiol. Biomarkers Prev.* **16**(10), 2048–2057 (2007).
17. L. C. Chen et al., "The potential of label-free nonlinear optical molecular microscopy to non-invasively characterize the viability of engineered human tissue constructs," *Biomaterials* **35**(25), 6667–6676 (2014).
18. J. V. Rocheleau et al., "Quantitative NAD(P)H/flavoprotein autofluorescence imaging reveals metabolic mechanisms of pancreatic islet pyruvate response," *J. Biol. Chem.* **279**(30), 31780–31787 (2004).
19. J. V. Rocheleau et al., "Pancreatic islet β-cells transiently metabolize pyruvate," *J. Biol. Chem.* **277**(34), 30914–30920 (2002).
20. W. Hu et al., "Nonlinear optical microscopy for histology of fresh normal and cancerous pancreatic tissues," *PLoS One* **7**(5), e37962 (2012).
21. W. Hu and L. Fu, "Simultaneous characterization of pancreatic stellate cells and other pancreatic components within three-dimensional tissue environment during chronic pancreatitis," *J. Biomed. Opt.* **18**(5), 056002 (2013).
22. A. Tuer et al., "Nonlinear multicontrast microscopy of hematoxylin-and-eosin-stained histological sections," *J. Biomed. Opt.* **15**(2), 026018 (2010).
23. J. Chen et al., "Multiphoton microscopic imaging of histological sections without hematoxylin and eosin staining differentiates carcinoma in situ lesion from normal oesophagus," *Appl. Phys. Lett.* **103**(18), 183701 (2013).
24. A. H. Fischer et al., "Hematoxylin and eosin staining of tissue and cell sections," *Cold Spring Harb. Protoc.* **3**(5), 1–2 (2008).
25. S. Zhuo et al., "Multimode nonlinear optical imaging of the dermis in ex vivo human skin based on the combination of multichannel mode and Lambda mode," *Opt. Express* **14**(17), 7810–7820 (2006).
26. A. Grapin-Botton, "Ductal cells of the pancreas," *Int. J. Biochem. Cell Biol.* **37**(3), 504–510 (2005).
27. P. Bedossa et al., "Quantitative estimation of the collagen content in normal and pathologic pancreas tissue," *Digestion* **44**(1), 7–13 (1989).
28. L. D. Thompson et al., "Mucinous cystic neoplasm (mucinous cystadenocarcinoma of low-grade malignant potential) of the pancreas: a clinicopathologic study of 130 cases," *Am. J. Surg. Pathol.* **23**(1), 1–16 (1999).
29. M. Erkan et al., "The activated stroma index is a novel and independent prognostic marker in pancreatic ductal adenocarcinoma," *Clin. Gastroenterol. Hepatol.* **6**(10), 1155–1161 (2008).
30. A. L. Cubilla and P. J. Fitzgerald, "Morphological patterns of primary nonendocrine human pancreas carcinoma," *Cancer Res.* **35**(8), 2234–2248 (1975).
31. M. B. Cohen et al., "Brush cytology of the extrahepatic biliary tract: comparison of cytologic features of adenocarcinoma and benign biliary strictures," *Mod. Pathol.* **8**(5), 498–502 (1995).
32. E. G. B. Fritcher et al., "Identification of malignant cytologic criteria in pancreatobiliary brushings with corresponding positive fluorescence in situ hybridization results," *Am. J. Clin. Pathol.* **136**(3), 442–449 (2011).
33. M. B. Pitman et al., "Cytological criteria of high-grade epithelial atypia in the cyst fluid of pancreatic intraductal papillary mucinous neoplasms," *Cancer Cytopathol.* **122**(1), 40–47 (2014).

Youting Chen is an associate chief physician working in the Department of Hepatobiliary Surgery, the First Affiliated Hospital of Fujian Medical University, China. His major research field is the diagnosis and treatment of liver, biliary, and pancreatic diseases.

Jing Chen is a postgraduate student of the Institute of Laser and Optoelectronics Technology, Key Laboratory of Optoelectronic Science and Technology for Medicine of the Ministry of Education at Fujian Normal University. His tutor is Xiaoqin Zhu.

Hong Chen is a pathologist working in the Department of Pathology, the First Affiliated Hospital of Fujian Medical University, China. Her main research interests are concentrated upon the mechanism of tumor genesis and progress.

Zhipeng Hong is a postgraduate student of the Institute of Abdominal Surgery, the First Affiliated Hospital of Fujian Medical University, China. His tutor is Zheng Shi, MD, professor, master tutor and chief physician of the Department of Hepatobiliary Surgery. His major research field is the diagnosis and treatment of liver, biliary, and pancreatic tumors.

Xiaoqin Zhu is an associate professor working at the Key Laboratory of OptoElectronic Science and Technology for Medicine of the Ministry of Education at Fujian Normal University. Her main research interests are focused on nonlinear spectroscopy and biomedical imaging.

Shuangmu Zhuo is an associate professor working at the Key Laboratory of OptoElectronic Science and Technology for Medicine

of the Ministry of Education at Fujian Normal University. His main research interests are concentrated upon nonlinear spectroscopy and biomedical imaging.

Yanling Chen is a professor, doctorial tutor, and chief physician in the Department of Hepatobiliary Surgery, the Affiliated Union Hospital of Fujian Medical University, China. His research field is the diagnosis and treatment of liver, biliary, and pancreatic tumors.

Jianxin Chen is a professor and director of Key Laboratory of Optoelectronic Science and Technology for Medicine, Ministry of Education, and vice secretary general of Chinese Optical Society. His research areas are application of depth-resolved nonlinear spectral imaging for determining the pathology of epithelial tissue based on two-photon excited autofluorescence and second-harmonic generation and application of multimode nonlinear optical imaging for evaluating physiological and pathological states of tissues.